Schroeder et al.
Force-dependent detachment of kinesin-2 biases track switching at cytoskeletal filament intersections

Supporting Material

Supporting Materials and Methods

Protein Preparation. Rabbit muscle G-actin was purified (1) and used to assemble F-actin along with Alexa 647-actin (Invitrogen, Inc.), and biotin-actin (Cytoskeleton, Inc.) at 1 μM total actin monomer concentration with a ratio of 21:15:1 or 20:5:1 G-actin:Alexa 647:biotin; filaments were stabilized with 1.1 μM rhodamine phalloidin (Invitrogen, Inc.). MTs were prepared from unlabelled tubulin, rhodamine-tubulin, and biotin-tubulin at 45 μM tubulin dimer with a ratio of 50:2:1.5 of tubulin dimer:rhodamine:biotin and stabilized with 40 μM Taxol (reagents from Cytoskeleton, Inc.).

A truncated kinesin-1 heavy chain construct (560 amino acids) fused to GFP was expressed and purified (2). Recombinant myosin-V-HMM (3) was tagged with FLAG-tag and 6xHis affinity sequences at the N-terminus and GFP at the C-terminus and expressed using the pFastBac HT vector (Invitrogen, Inc.) in Sf9 cells, then purified by FLAG affinity chromatography. DNAs for the motor subunits of Xenopus kinesin-2 were amplified by PCR from RNA isolated from Xenopus melanophores using primers designed against the published sequences of Xenopus kinesin-2 subunits (NM_001090799.1 GI:148228463, and NM_001088020.1 GI:148231166). For co-expression of kinesin-2 subunits in baculovirus, Xklp3A-6xHis and Xklp3B DNA were cloned into the pFastBac Dual Vector (Invitrogen, Inc.) downstream of the PH (Xklp3A-6xHis) or AcMNPV p10 (Xklp3B) promoters. A GFP tag was introduced at the C-terminus of XKlp3B. XKlp3A-6His/XKlp3B-GFP heterodimers were expressed in Sf9 cells using the Bac-to-Bac Baculovirus Expression System (Invitrogen, Inc.), and purified by chromatography on Ni-NTA agarose (Qiagen Corp.) as described (4). Motor protein concentrations were initially determined by gel densitometry in comparison to a BSA dilution series run on the same gel, and verified by western blot versus a standard curve of purified GFP-labeled Myo1c (provided by Elizabeth Feeser and Michael Ostap).

In Vitro Filament Switching Assays. Flow chambers (~10 μL volume) were assembled to make two perpendicular crossed flow paths with MTs and AFs bound to the cover slips via biotin-streptavidin linkers as described (5). First, cover slips were blocked with 1 mg/mL biotinylated-BSA (Sigma) in motility buffer (MB: 80 mM PIPES, 1 mM $MgCl_2$, 1 mM EGTA, pH 7.5) and then rinsed with wash buffer (WB, MB supplemented with 1 mg/mL BSA, 20 μM Taxol, and 10 mM DTT), followed by incubation with 2 mg/mL streptavidin. Rhodamine-labeled, biotinylated MTs (0.45 μM tubulin dimer) in MB with 20 μM Taxol were flowed into the chamber in the *y*-direction and rhodamine phalloidin-labeled, biotinylated, Alexa-647-labeled AFs (50 nM actin monomer) in MB with 20 μM Taxol were flowed into the chamber in the *x*-direction. MTs are termed "underpasses" and AFs termed "overpasses" because the MTs are closer to the glass. Chambers were blocked with 5 mg/mL casein, 20 μM Taxol, and 10 mM DTT in MB, then rinsed with MB supplemented with 6 mg/mL BSA, 24 μM Taxol, 1.2 mM DTT, 71 μg/mL CaM, 2.4 mM ATP, 12 mM phosphocreatine, 0.54 mg/mL creatine phosphokinase, 3.6 mg/mL glucose, 120 μg/mL glucose oxidase, and 48 μg/mL catalase.

Motor-bound beads were introduced into the flow chamber, which was then sealed with vacuum grease.

Filaments and beads were viewed by epifluorescence microscopy on an inverted microscope (Olympus, Inc. IX71). Beads were captured with an optical trap and positioned onto either MTs or AFs near intersections. Image sequences were collected at 1 frame/s using a CCD camera (Hamamatsu, Inc., ORCA-ER C4742-95-12ER) or an electron multiplying CCD camera (Andor, Inc., IXON DV887DCS-BV). The optical trap setup with water immersion lenses (objective: UPlanApo/IR 60x, condenser: PlanApoUV 60x) was as described (6) but with only one trap. Trap stiffness was measured by fitting a Lorentzian to the power spectrum of thermal oscillations of a trapped bead (7). For force measurements, quadrant photo-diode (QPD) data were anti-alias filtered at 1 kHz and digitized at 2 kHz. In a given experiment, force measurements were typically performed on different beads from those used for the track switching measurements to avoid motor damage due to prolonged exposure to the infrared laser light. Data acquisition and analysis were performed using custom software written in LabVIEW (National Instruments), NIH ImageJ and MATLAB (The Mathworks).

Statistical Modeling. A model was developed to describe the probabilistic nature of track switching based on the stochastic nature of motor attachment and detachment as previously described (5). This model follows from two main premises: 1) the number of actively engaged motors, n, out of a maximum number of motors available for engagement, N, from each motor group follows a steady-state binomial distribution,

$$P(n) = \frac{N!}{n!(N-n)!} p^n (1-p)^{N-n} \qquad \text{Eq. 1}$$

where p is the "engagement ratio," the probability that an individual motor is producing force, and 2) the bead exits the intersection on the track corresponding to the motor team exerting the greater force. The resulting probabilities for exiting along either AFs or MTs were fit using an S-shaped curve of the form, $y = 100/(1+e^{-(x-b)/c})$. The independent variable, x, is the logarithm of the kinesin-2:myosin-V maximum force ratio. The only adjustable parameters in fitting this simple statistical model to the data are the two engagement ratios, $p_{\text{kinesin-2}}$ and $p_{\text{myosin-V}}$. The unitary stall force for each motor was based on experimental data (Figs. 1,2).

We next tested the effect of force-dependent dissociation kinetics by adapting a steady state model for vesicular transport by oppositely-directed motors (8) to the switching assays. In the place of minus- and plus-end directed motors, we considered a tug-of-war between MT- and AF-based motors. Force-dependent unbinding rate in this model is expressed as:

$$\epsilon(F) = \epsilon_0 exp(|F|/F_d) \qquad \text{Eq. 2}$$

where F is the applied force exerted by a load such as a competing team of motors and F_d is a parameter, termed the 'detachment force', describing the force sensitivity for detachment. Although detachment rate for kinesin is not necessarily such a simple function of force (9), this model captures a qualitative difference among the motor types according to the ratio of F_d to stall force. e.g. F_d/F_{stall} is lower for kinesin-2 than for myosin V (see below).

To examine the role of transient binding and dissociation kinetics at cytoskeletal intersections, we also performed dynamic Monte Carlo simulations (8). To simulate competing motor teams at filament intersections, the binding rate for motors in this model was assumed to be zero when the bead is farther than an interaction distance, D_{int}, from the corresponding filament. Thus, both types of motors only engage near the intersection.

Supporting Tables, Figures, and Movies

	Kinesin-2	Myosin-V	Dynein
Engagement Ratio, p Starting on actin filament	0.7	0.7	0.85
Engagment Ratio, p Starting on microtubule	0.56	0.7	0.85
Moving Maximum Force, $F_{mm}\ (pN)$	3.8	2	1

(a) Binomial Model parameters

		Kinesin-2	Myosin-V	Dynein
Stall Force,	$F_S\ (pN)$	5	2	1.1
Detachment Force,	$F_d\ (pN)$	2	1	0.75
Unbinding Rate,	$\varepsilon_0\ (s^{-1})$	2.5	1.3	0.27
Binding Rate, Steady-state - Starting on actin filament	$\pi_0\ (s^{-1})$	5	5	0.95
Binding Rate, Steady-state - Starting on microtubule	$\pi_0\ (s^{-1})$	2.5	5	0.95
Binding Rate, Dynamic model	$\pi_0\ (s^{-1})$	3.5	5	0.95
Forward Velocity,	$v_F\ (nm/s)$	625	400	500
Back Velocity,	$v_B\ (nm/s)$	4	4	72

(b) Force-dependent dissociation model parameters

Table S1. Model Parameters. Parameters were chosen based on available single-molecule data. The parameters for kinesin-2 were based on measurements in the current study and (10, 11). Myosin-V parameter values were based on the current study, and values from (5). Parameters for dynein were taken from (8). For fitting to the data, the free parameters were (a) the engagement ratio in the binomial model, and (b) the binding rate in the force-dependent dissociation model.

	Motor 1	Motor 2
Stall Force, $F_S\ (pN)$	1	1
Detachment Force, $F_d\ (pN)$	0.5, 0.25	0.5, 0.25
Unbinding Rate, $\varepsilon_0\ (s^{-1})$	1	1
Binding Rate, $\pi_0\ (s^{-1})$	5, 2.5	5, 2.5
Forward Velocity, $v_F\ (nm/s)$	500	500
Back Velocity, $v_B\ (nm/s)$	5	5

Table S2. Force-dependent dissociation model sensitivity analysis parameter values. To test the influence of the detachment force and binding rate on track switching, we simulated a tug-of-war between two groups of 1-4 identical motors (1-8 for ΔNm_{12}). Then the detachment force or binding rate were changed for one or both of the motors.

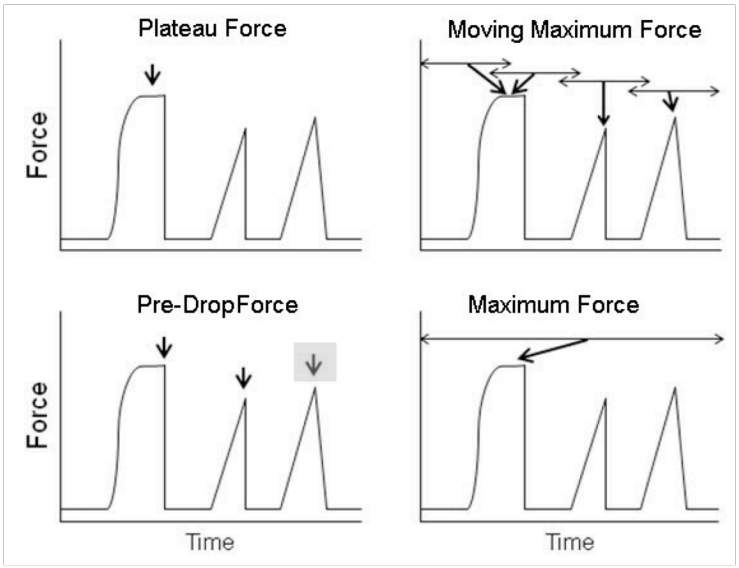

Figure S1. Graphical representation of the definitions used to determine force measurements from optical trap traces. We measured plateau forces for kinesin-1 and kinesin-2 from stalls with durations ≥ 70 ms followed by detachment and return to baseline. As noted in the Materials and Methods section, changing the stall duration to ≥ 100 ms did not appreciably change the plateau force values determined. Stall events for myosin-V were more robust, so no threshold was necessary. To calculate moving maximum force we used a sliding filter as described in the Methods section. Pre-drop forces were defined as the force value immediately preceding the point of velocity reversal of at least 20 μm/s towards baseline; note that the peak indicated by the arrow in the gray box would not be included by this criterion. Maximum force was identified as the maximum force measured for a given motor concentration.

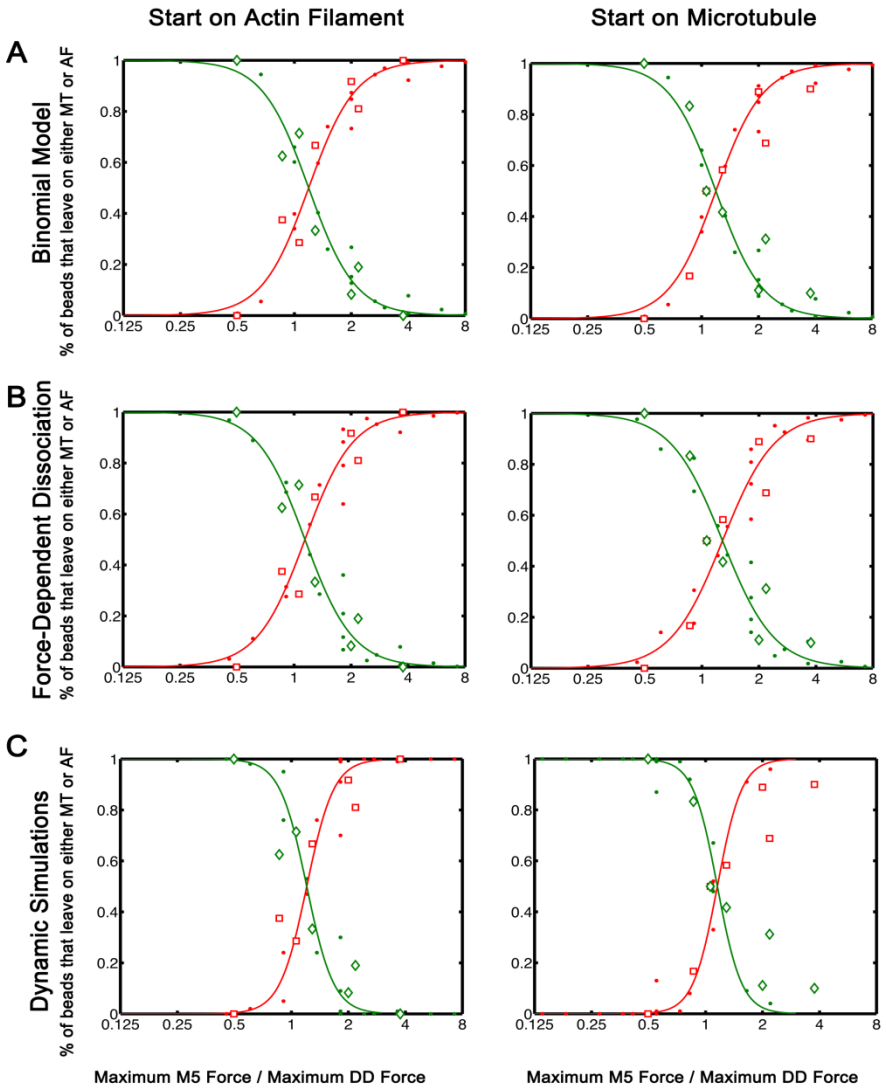

Figure S2. Model of filament switching driven by dynein-dynactin and myosin-V. Cargos driven by dynein and myosin-V was less sensitive to the starting filament than for cargos driven by kinesin-2 and myosin-V. Several parameters contribute to switching kinetics. The unitary stall force for dynein is 1 pN compared to 5 pN for kinesin-2, meaning that for similar loads exerted by myosin-V, the load is shared among more dynein motors than a similar tug of war between myosin-V and kinesin-2. Thus, the change in the load experienced by each motor when one motor in the team detaches is less for dynein than kinesin-2. In addition, the ratio of the detachment force to the stall force is 0.4 for kinesin-2 and 0.68 for dynein, indicating that the detachment of kinesin-2 is more dependent on force than dynein. Accordingly, forces exerted by myosin-V will accelerate detachment for kinesin-2 to a greater extent than dynein.

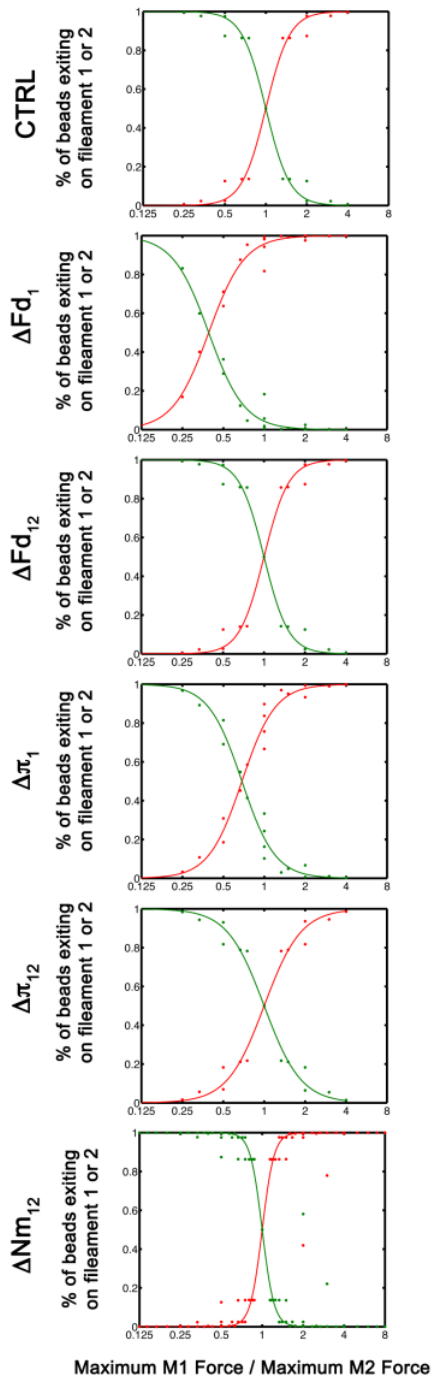

	Transition Force Ratio	Transition Slope (*10^{-3})
CTRL	1.00	50.8
ΔF_{d1}	0.390	76.0
ΔF_{d12}	1.00	52.0
$\Delta \pi_{0,1}$	0.685	70.4
$\Delta \pi_{0,12}$	1.00	78.0
$\Delta N m_{12}$	1.00	25.2

Figure S3. Sensitivity of the steady-state force-dependent model to detachment force and binding rate. In the steady state model, the detachment force dramatically affects the transition force ratio (a), while having little effect on the transition slope (b/4) where a and b are determined by fitting the data to the curve P=1/(1-exp(-(x-a)/b)). Decreasing the binding rate for one motor shifts the transition force ratio, while decreasing the binding rate for both motors leads to a sharper transition as evidenced by increasing the transition slope. Increasing the total number of motors also increases the transition slope.

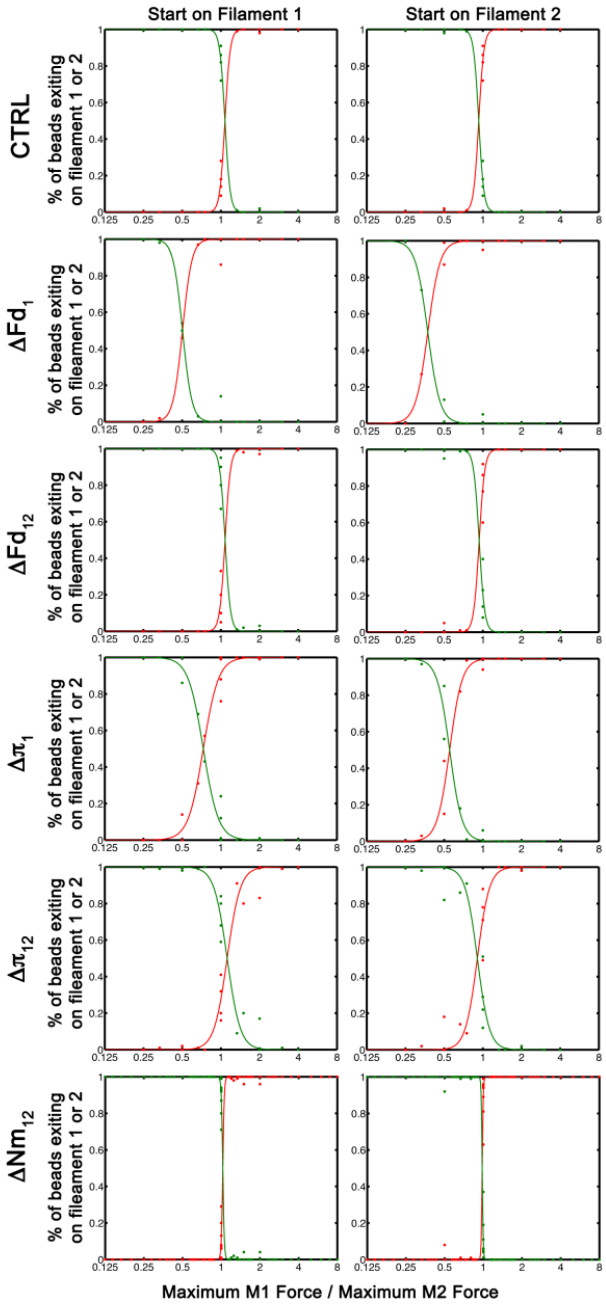

	Start on Filament 1		Start on Filament 2	
	Transition Force Ratio	Transition Slope ($*10^{-3}$)	Transition Force Ratio	Transition Slope ($*10^{-3}$)
CTRL	1.03	5.06	0.969	5.06
ΔF_{d1}	0.742	9.10	0.652	12.0
ΔF_{d12}	1.03	5.24	0.972	5.39
$\Delta \pi_{0,1}$	0.873	14.7	0.772	12.2
$\Delta \pi_{0,12}$	1.05	12.7	0.958	11.7
$\Delta N m_{12}$	1.01	1.44	0.992	0.974

Figure S4. Sensitivity of the dynamic model to detachment force and binding rate. Decreasing either the detachment force or the binding rate of one motor shifts the transition force ratio, and leads to asymmetry with respect to the starting filament. As in the steady state model, the transition rate is sensitive to the binding rate and number of motors but not the detachment force.

Movie S1. Motor-driven switching at a cytoskeletal intersection. Myosin-V and kinesin-2 motors were bound to polystyrene beads. A motor-bound bead was positioned near a cytoskeletal intersection assembled in vitro from a microtubule and an actin filament. The bead initially travels along the microtubule, driven by kinesin-2, but switches to motility along the actin filament driven by myosin-V.

Supporting References

1. Pardee, J. D., and J. A. Spudich. 1982. Purification of muscle actin. Methods Cell Biol 24:271-289.
2. Pierce, D. W., and R. D. Vale. 1998. Assaying processive movement of kinesin by fluorescence microscopy. Methods Enzymol 298:154-171.
3. Homma, K., J. Saito, R. Ikebe, and M. Ikebe. 2000. Ca(2+)-dependent regulation of the motor activity of myosin V. J Biol Chem 275:34766-34771.
4. Hancock, W. O., and J. Howard. 1998. Processivity of the motor protein kinesin requires two heads. J Cell Biol 140:1395-1405.
5. Schroeder, H. W., 3rd, C. Mitchell, H. Shuman, E. L. Holzbaur, and Y. E. Goldman. 2010. Motor Number Controls Cargo Switching at Actin-Microtubule Intersections In Vitro. Curr Biol.
6. Takagi, Y., E. E. Homsher, Y. E. Goldman, and H. Shuman. 2006. Force generation in single conventional actomyosin complexes under high dynamic load. Biophys J 90:1295-1307.
7. Svoboda, K., and S. M. Block. 1994. Force and velocity measured for single kinesin molecules. Cell 77:773-784.
8. Muller, M. J., S. Klumpp, and R. Lipowsky. 2008. Tug-of-war as a cooperative mechanism for bidirectional cargo transport by molecular motors. Proc Natl Acad Sci U S A 105:4609-4614.
9. Nishiyama, M., H. Higuchi, and T. Yanagida. 2002. Chemomechanical coupling of the forward and backward steps of single kinesin molecules. Nat Cell Biol 4:790-797.
10. Muthukrishnan, G., Y. Zhang, S. Shastry, and W. O. Hancock. 2009. The processivity of kinesin-2 motors suggests diminished front-head gating. Curr Biol 19:442-447.
11. Brunnbauer, M., F. Mueller-Planitz, S. Kosem, T. H. Ho, R. Dombi, J. C. Gebhardt, M. Rief, and Z. Okten. 2010. Regulation of a heterodimeric kinesin-2 through an unprocessive motor domain that is turned processive by its partner. Proc Natl Acad Sci U S A 107:10460-10465.